

# Mesenchymal Stem Cell–Laden In Situ–Forming Hydrogel for Preventing Corneal Stromal Opacity

Yinan Liu, PhD, MD,\*† and Jing Hong, PhD, MD\*†

**Purpose:** The aims of this study were to construct a mesenchymal stem cell (MSC)–laden in situ–forming hydrogel and study its effects on preventing corneal stromal opacity.

**Methods:** The native gellan gum was modified by high temperature and pressure, and the rabbit bone marrow MSCs were encapsulated before adding  $\text{Ca}^{2+}$  to initiate cross-linking. The effects of the hydrogel on 3D culture and gene expression of the rabbit bone marrow MSCs were observed in vitro. Then, the MSC–hydrogel was used to repair corneal stromal injury in New Zealand white rabbits within 28 days postoperation.

**Results:** The short-chain gellan gum solution has a very low viscosity ( $<0.1 \text{ Pa}\cdot\text{s}$ ) that is ideal for encapsulating cells. Moreover, mRNA expressions of 3D-cultured MSCs coding for corneal stromal components (decorin, lumican, and keratocan) were upregulated (by 127.8, 165.5, and 25.4 times, respectively) ( $P < 0.05$ ) on day 21 in vitro and were verified by Western blotting results. For the in vivo study, the corneal densitometry of the experimental group was ( $20.73 \pm 1.85$ ) grayscale units which was lower than the other groups ( $P < 0.05$ ). The MSC–hydrogel downregulated mRNA expression coding for fibrosis markers ( $\alpha$ -smooth muscle actin, vimentin, collagen type 5- $\alpha$ 1, and collagen type 1- $\alpha$ 1) in the rabbit corneal stroma. Furthermore, some of the 5-ethynyl-2'-deoxyuridine (EdU)-labeled MSCs integrated into the upper corneal stroma and expressed keratocyte-specific antigens on day 28 postoperation.

**Conclusions:** The short-chain gellan gum allows MSCs to slowly release to the corneal stromal defect and prevent corneal stromal opacity. Some of the implanted MSCs can integrate into the corneal stroma and differentiate into keratocytes.

**Key Words:** gellan gum, in situ cross-linking, mesenchymal stem cell, corneal stromal opacity, cell encapsulation

(*Cornea* 2024;43:609–626)

## INTRODUCTION

Corneal damage starts transforming growth factor- $\beta$ /small mothers against decapentaplegic (TGF- $\beta$ /Smad) signals making myofibroblasts secrete abnormal collagen fibers which leads to fibrosis of the stroma and manifests as permanent corneal stromal opacity.<sup>1</sup> It is the third most common cause of visual impairment worldwide after cataract and glaucoma.<sup>2</sup> In China, there are nearly 4 million patients troubled by severe visual impairment caused by corneal diseases with about 200,000 new cases reported yearly.<sup>3,4</sup> Keratoplasty is the only effective method to restore vision of those patients. However, owing to the extreme shortage of donors in China, only about 10% of them can finally receive keratoplasty.<sup>5</sup> Therefore, to find a new medical strategy against corneal stromal opacity has a profound significance.

Tissue engineering is a new opportunity for corneal opacity and stromal regeneration<sup>6</sup> and ideal seed cells are the key to success. Multiple studies have confirmed that mesenchymal stem cells (MSCs) and their exosomes are effective in treating corneal stromal opacity.<sup>7–10</sup> MSCs are well known in regenerative medicine for their ability to modulate the immune system.<sup>11</sup> Many animal studies have observed that with the administration of MSCs, certain inflammatory factors reduced, including TGF- $\beta$ , interleukin-6 (IL-6), and vascular endothelial growth factor, resulting in the inhibition of T and B lymphocytes.<sup>12–15</sup> Second, MSCs can reduce preexisting corneal scars by secreting cell factors such as hepatocyte growth factor and upregulating secretion of type V collagen by target cells to remodel the stroma.<sup>16–18</sup> Moreover, several authors showed that MSCs were capable of differentiating into functional keratocytes and producing new collagen both in vitro and in vivo which leads to corneal stromal regeneration.<sup>19–22</sup> However, MSCs showed poor stability with a low survival rate when transplanted alone into the cornea and often require repeated applications.<sup>23</sup> Therefore, it is important to construct a suitable scaffold material to carry MSCs and form a tissue-engineered corneal graft for effective transplantation.

Among all scaffold materials, hydrogels have attracted wide attention because of their sutureless application process. Hydrogels alone or together with cells as “repair patch” filling in corneal defects can be categorized into 2 classes: synthetic and naturally derived hydrogels. To name a few,

Received for publication June 15, 2023; revision received October 26, 2023; accepted December 6, 2023. Published online ahead of print January 30, 2024.

From the \*Department of Ophthalmology, Peking University Third Hospital, Beijing, China; and †Beijing Key Laboratory of Restoration of Damaged Ocular Nerve, Beijing, China.

Supported by the General Program of Beijing Municipal Natural Science Foundation (7222210).

The authors have no funding or conflicts of interest to disclose.

Supplemental digital content is available for this article. Direct URL citations appear in the printed text and are provided in the HTML and PDF versions of this article on the journal's Web site ([www.corneajrnl.com](http://www.corneajrnl.com)).

Correspondence: Jing Hong, PhD, MD, Department of Ophthalmology, Peking University Third Hospital, 49th North Garden Rd, Haidian District, Beijing 100191, China (e-mail: [hongjing196401@163.com](mailto:hongjing196401@163.com)).

Copyright © 2024 The Author(s). Published by Wolters Kluwer Health, Inc. This is an open access article distributed under the terms of the Creative Commons Attribution-Non Commercial-No Derivatives License 4.0 (CCBY-NC-ND), where it is permissible to download and share the work provided it is properly cited. The work cannot be changed in any way or used commercially without permission from the journal.

cyanoacrylates,<sup>24</sup> polyethylene glycol,<sup>25</sup> collagen,<sup>26,27</sup> fibrin,<sup>28</sup> alginate,<sup>29</sup> chitosan,<sup>16</sup> gelatin,<sup>30</sup> and decellularized extracellular matrix (ECM)<sup>31</sup> have been studied for corneal repair. Synthetic hydrogels are easy to customize and preferable in meeting certain desired properties, but they may not promote tissue regeneration.<sup>32</sup> Natural hydrogels are excellently biocompatible, but their mechanical stability is often inadequate.<sup>33</sup>

Gellan gum is a linear anionic polymer and an extracellular polysaccharide, which is actually a kind of ECM secreted by *Sphingomonas* sp. It is favored by biomedical research because of its desirable biocompatibility and the capability of drug release.<sup>34</sup> For ocular drug delivery studies, gellan gum has been used to load 1) levofloxacin hemihydrate or natamycin bilosomes to cure ocular bacterial<sup>35</sup> or fungal infection<sup>36</sup>, 2) triamcinolone acetonide nanoparticles for sustained delivery of triamcinolone acetonide into the anterior and posterior ocular tissues<sup>37</sup>, and 3) antiglaucoma drugs for long-term control of intraocular pressure.<sup>38,39</sup>

In this study, the native gellan gum was physically modified by high temperature and pressure, so that its long-chain structure was truncated to make it into liquid form under room temperature to encapsulate rabbit bone marrow mesenchymal stem cells (Rb-BMSCs) evenly and safely. The short-chain gellan gum loaded with Rb-BMSCs was dripped into the “pit” of rabbit corneal stromal defect and crosslinked in situ under the application of  $\text{Ca}^{2+}$ . It forms a “repair patch” that just fits the shape of the corneal stromal defect, aiming to prevent scar formation and preserve vision of those with an injured cornea.

## MATERIALS AND METHODS

### Preparation of Short-Chain Gellan Gum

Gellan gum powder (Gelzan, Sigma-Aldrich) and anhydrous glucose (Sigma) were dissolved in 80°C deionized water under constant electromagnetic stirring to acquire 0.75% gellan gum–5% glucose isotonic solution. Then, the solution was transferred to a high-temperature and high-pressure (121°C, 0.1 MPa) incubator and processed for 20 minutes before cooling to room temperature to get the short-chain gellan gum solution. A bandage contact lens (PureVision, Bausch & Lomb) was immersed in 0.1M  $\text{CaCl}_2$  (Sigma) solution for later use. Two hundred  $\mu\text{L}$  of short-chain gellan gum solution was dropped into a silicon mold of 8 mm diameter and 2 mm depth. Then the solution’s surface was gently covered by the contact lens coated with  $\text{Ca}^{2+}$ . After cross-linking for 3 minutes, the contact lens was removed and the gel was inverted and rinsed with phosphate-buffered saline (PBS) (HyClone) free of  $\text{Ca}^{2+}/\text{Mg}^{2+}$  for 3 times.

### Characterization of Solutions and Hydrogels

#### Rheology of the Native and Short-Chain Gellan Gum Solution

The experiments were conducted according to previously published articles<sup>40,41</sup> using a Kinexus super rota-

tional rheometer (Malvern Instruments Ltd, UK). The experiment to measure the viscosity of the short-chain gellan gum solution processed by different incubation time was conducted at room temperature. The temperature-dependent experiments were conducted in a range from 10 to 45°C. The sol–gel transition point was determined by the crossing of the storage modulus ( $G'$ ) and loss modulus ( $G''$ ) curves. In addition, frequency-dependent rheology was tested at room temperature, with a strain rate of 2%. Oscillation strain-dependent phase angle was recorded with the shear strain ranging from 1% to 100% at room temperature. Shear-dependent and time-dependent viscosity changes were measured at room temperature.

### Scanning Electron Microscope Observation

Specimens of 0.75% short-chain gellan gum and 0.75% native gellan gum were lyophilized by a freeze-drying machine (CHRIST, Martin Christ, Germany) for 72 hours. Then the samples were cross-sectioned and fixed on a grid attached with carbon tape. After being coated in vacuum by plasma sputter, the sample surfaces were imaged by a scanning electron microscope (Quattro S EDAX ELECT PIUS, Thermo Fisher).

### Gel Permeation Chromatography

Molecular values of the native and short-chain gellan gum were measured by gel permeation chromatography (Agilent 1260). Chromatographic conditions were set as follows: column: Ultrahydrogel Linear 300 mm  $\times$  7.8 mmid; mobile phase: 0.1M sodium nitrate; flow rate: 0.5 mL/min.

### Light Transmittance

Specimens of 0.75% short-chain gellan gum were trephined to 6 mm diameter using a corneal surgical trephine (Shiqiang, China). Then the specimens were carefully transferred into a 96-well plate, and the absorbance ( $A$ ) in the 400 to 800 nm range was detected by a microplate reader (Epoch2, BioTek), with light transmittance ( $T$ ) =  $10^{-A}$ .

### Young Modulus

To prepare short-chain gellan gums with different stiffnesses, the cross-linking time by  $\text{Ca}^{2+}$  was controlled. After 1, 2, 3, 5, 7, 10, 15, 20, and 25 minutes, the bandage lens coated with  $\text{Ca}^{2+}$  was removed, respectively. Then the gel was inverted and rinsed 3 times with PBS. Fresh rabbit eyeballs were enucleated and the central cornea was trephined to 8 mm diameter. The corneal epithelium, Bowman membrane, Descemet membrane, and corneal endothelium were removed under a microscope, and the corneal stroma was rinsed with PBS for 3 times. The above specimens were placed on the sample table and scanned by an atomic force microscope (HORIBA, AIST NT) with the scanning rate of 2  $\mu\text{m}/\text{s}$ .<sup>42</sup> The Young modulus was calculated by a custom software MATLAB (ver. 2013; Mathworks).

### In Vitro Dissolvement Rate

Dissolvement of the short-chain gellan gum was observed within 21 days and measured according to the previously published literature<sup>43</sup> and is briefly described as

follows: First, all samples were lyophilized by a freeze-drying machine for 7 days to thoroughly remove the moisture and weighed (W0). Then, the samples were placed in a plastic tube and immersed in 10 mL of PBS under 7.4 pH. The tube was then transferred to a 37°C incubator with a shaking speed of 60 rpm for 21 days. The supernatant was replaced every day. On days 1, 3, 5, 7, 14, and 21, the supernatant was removed and the residual hydrogels were collected at the bottom of the tube. The collected gels were lyophilized for another 7 days and weighed (W1).

In vitro dissolution rate of the short-chain gellan gum (%) =  $(W0 - W1)/W0 \times 100$ .

### Release Property of MSC-Hydrogels

For determining the cell release behavior of the hydrogel, the prepared MSC-hydrogels (refer to the section Rb-BMSCs Encapsulation in Hydrogels) together with 5 mL of PBS were placed in a pipe and maintained at 37°C in an incubator with a shaking speed of 500 rpm. The supernatant was replaced and collected every day until the seventh day. A bicinchoninic acid protein assay kit (Beyotime, China) was used to quantify the total protein of the released MSCs over time. The total protein of MSCs in the hydrogel was measured in the preliminary experiment and was about 654.5 µg.

### Adhesion Force Between the Short-Chain Hydrogel and Cornea

The adhesion force between the short-chain hydrogel and cornea was performed according to a previously published article<sup>44</sup> and was detected using an extensometer (Lloyd Instruments, UK). Twelve rabbit eyes were enucleated, and the cornea was trephined with an 8-mm diameter trephine. A 3D printer (Formlabs) was used to print a sleeve 100 µm lower than a 3-mm diameter trephine to get a fixed depth trephine (see Figure, Supplemental Digital Content 1, <http://links.lww.com/ICO/B622>). Then, the central cornea was trephined and removed with a lamellar keratome, and the basal corneal stroma was polished with a corneal rust ring remover (Alger) for 30 seconds, forming a corneal defect of 3 mm diameter and 100 µm depth. Then, 20 µL of short-chain gellan gum solution was dripped to the defect, and a bandage contact lens coated with Ca<sup>2+</sup> was applied to cover the cornea. After 3 minutes, the contact lens was removed and the cornea was washed with PBS free of Ca<sup>2+</sup>/Mg<sup>2+</sup>. Two cardboards were glued respectively to the top and bottom of the above complex and clamped on the extensometer. Then, the gel plug was pulled in opposite vertical directions until it was detached. The force required to detach the gel from the corneal bed was recorded and analyzed.

### Isolation, Culture, and Identification of Rb-BMSCs

#### Isolation and Culture of Rb-BMSCs

Ethics approval for this study was obtained from the Ethics Committee of Peking University Third Hospital. Rb-BMSCs were obtained from the tibia of adult New Zealand

white rabbits as previously described.<sup>45</sup> The harvested cells were resuspended in Dulbecco modified Eagle medium (Corning) containing 10% fetal bovine serum (Gibco), 100 U/mL penicillin, and 100 µg/mL streptomycin (Gibco). Then, the cells were seeded in 6-well plates and cultured in a cell incubator containing 5% CO<sub>2</sub> at 37°C. The medium was changed every 2 days.

#### Labeling Rb-BMSCs by 5-ethynyl-28'-deoxyuridine

The method of labeling Rb-BMSCs by EdU was referred to the EdU-488 Cell Proliferation Detection Kit's (Beyotime, China) instructions. EdU was diluted and added to 80% confluent cultures to obtain a final concentration of 10 µM. The cells were incubated at 37°C for 24 hours and washed twice with PBS. Then, the click reaction solution was added to the cells and incubated at room temperature for another 30 minutes away from light.

#### Identification of Rb-BMSCs

##### *Adipogenic, Osteogenic, and Chondrogenic Differentiation Assay*

After growing to 70% confluence, the pluripotency validation of MSCs was tested according to procedures described before.<sup>46</sup> The culture medium was changed every 2 days until Oil Red O (Solarbio, China) staining, Alizarin Red S (Solarbio, China) staining, and Alcian blue (Solarbio, China) staining were performed 2 weeks later.

##### *Flow Cytometry*

Flow cytometry was performed to identify the molecular phenotype of Rb-BMSCs. The cells were prepared as previously described<sup>45</sup> and were incubated with primary antibodies (CD34 1:100 and CD29 1:100) or isotype control at room temperature for 15 minutes. Fluorescent cell analysis was performed with an FACSCalibur cytometer (LSR Fortessa, BD Biosciences), and the results were analyzed by BD FACSDiva software v7.0 (BD Biosciences).

### Rb-BMSCs Encapsulation in Hydrogels

The cultured Rb-BMSCs (Passage 0) were gently mixed with 0.75% short-chain gellan gum solution cooled to room temperature and 0.75% native gellan gum solution cooled to 39°C to obtain homogeneous solutions of 10<sup>6</sup> cells/mL. Two hundred microliters of MSC solution was dropped into a silicon mold of 8 mm diameter and 2 mm depth. Then, the solution's surface was covered by a bandage contact lens coated with Ca<sup>2+</sup>. After cross-linking for 3 minutes, the contact lens was removed and the MSC-hydrogel was inverted and rinsed with PBS free of Ca<sup>2+</sup>/Mg<sup>2+</sup> for 3 times. The MSC-hydrogel was then transferred to the central slide of a confocal plate. The cell culture medium was added to submerge the gel. Cells and cell masses were counted per 10 × 10 field of view using an optical microscope. The gel was cultured in a cell incubator containing 5% CO<sub>2</sub> at 37°C and the medium was changed every 2 days (Fig. 1).

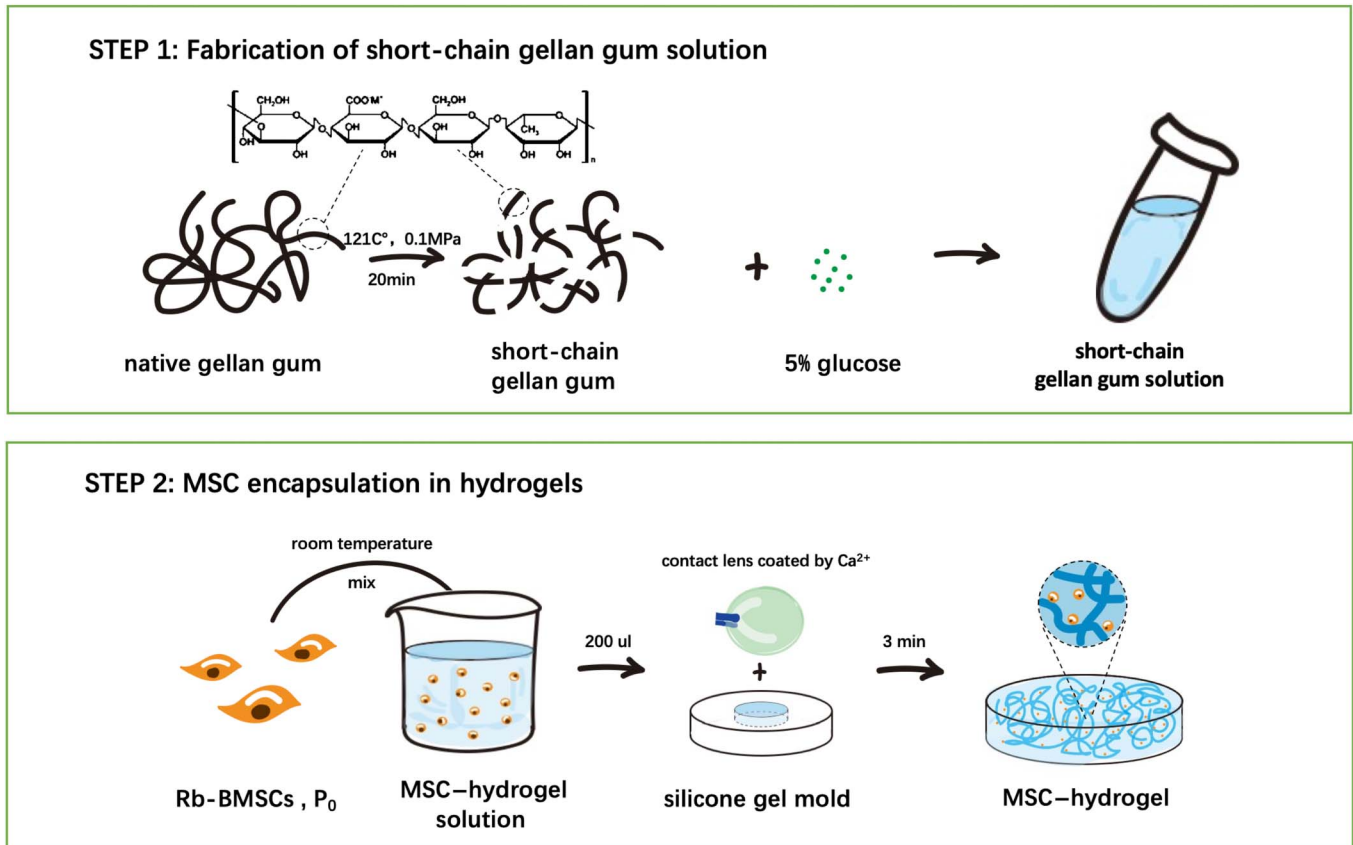


**FIGURE 1.** Schematic drawing of the preparation of the short-chain gellan gum–MSC hydrogel.

## In Vitro Study

### Cell Viability Assay

The morphology of cells in the hydrogels was observed by an optical microscope. A CCK8 cell proliferation and toxicity assay kit (Appligen, China) was used to detect the metabolic activity of cells. After being cultured for 7, 14, and 21 days, the supernatant was removed and 1 mL of fresh medium with 200  $\mu$ L of CCK8 reagent was added. After incubating at 37°C for 3 hours, the supernatant was transferred to a 96-well plate, and the absorbance (OD value) was measured at 450 nm wavelength by a microplate reader (Epoch2, BioTek). The metabolic activity of cells was marked as “OD sample–OD blank”.

### Live and Dead Staining

A Calcein/PI cell viability and cytotoxicity test kit (Beyotime, China) was used to detect live/dead cells. After being cultured in hydrogels for 7, 14, and 21 days, the gels were washed with PBS for 3 times. One milliliter of Calcein acetoxymethyl/propidium iodide (AM/PI) working solution was added to the gel and cocultured at 37°C for 30 minutes. A confocal microscope (LSM 510 META, Carl Zeiss, Germany) was used to photograph the images with z-stack mode. The Fiji ImageJ 2.3.0 software with cell count mode was used to count the cells in green/red channels and calculate the proportion of the living cells.

### Gene Expression

The relative gene expression level of short-chain gellan gum–cultured MSCs was detected by reverse transcription–quantitative polymerase chain reaction (RT–qPCR). On day 0 and day 21 of coculture, total RNA was extracted by a total RNA extraction kit (Solarbio, China). SYBR master mix (Thermo) was used for real-time fluorescence quantitative PCR detection (7500 Real-Time PCR System, Thermo). The target genes code for main components of corneal stroma include collagen type I- $\alpha$ 1 (COL1A1), lumican (LUM), decorin (DCN), biglycan (BGN), and keratocan (KERA).<sup>47</sup> The gene expression was adjusted by ACTB (coding for  $\beta$ -actin) used as a reference gene. The primer design is shown in Supplemental Digital Content 2 (see Table, <http://links.lww.com/ICO/B624>).

### Western Blotting

To verify the protein synthesis related to the above upregulated mRNAs, the total protein of the short-chain gellan gum–cultured MSCs was extracted respectively on day 0 and day 21 of coculture by a total protein extraction kit (Appligen, China) and quantified by a bicinchoninic acid protein quantitative kit (Appligen, China). The loading quantity of the protein sample was 20  $\mu$ g. 10% sodium dodecyl sulfate polyacrylamide gel electrophoresis–separated proteins were electrophoretically transferred to a nitrocellulose (NC) membrane (Appligen,

China) which was then incubated with 1:500 lumican rabbit polyclonal antibody (Beyotime, China, AF7401)/1:500 DCN rabbit polyclonal antibody (Beyotime, China, AF6693)/1:500 KERA rabbit monoclonal antibody (Boster, China, PB0694). Glyceraldehyde phosphate dehydrogenase was used as a reference protein, and 1:1000 glyceraldehyde phosphate dehydrogenase mouse monoclonal antibody (Beyotime, China, AF5009) was used. The bands on the NC film were semiquantitatively analyzed by Fiji ImageJ 2.3.0 software.

## In Vivo Study

### Ocular Surface Transplantation of MSC-Hydrogels

Male New Zealand white rabbits, aged 8 to 12 weeks and weighed 1.5 to 2.0 kg, were purchased from Beijing Fuhao Experimental Animal Center. This animal experiment was approved by the Animal Ethics Review Committee of Peking University Third Hospital (No. 2023043-02). The EdU-labeled MSCs were mixed with short-chain gellan gum solution under room temperature to obtain a cell density of  $10^6$  cells/mL. Forty-eight rabbits were randomly divided into 3 groups: MSC-hydrogel group using short-chain gellan gum containing Rb-BMSCs, hydrogel group using short-chain gellan gum, and control group with no treatment. Tiletamine + zolazepam (Zoletil, Virbac, France) was intramuscularly injected for anesthesia (5 mg/kg). The animal model of corneal stromal opacity was obtained according to previous literature,<sup>48</sup> and the preparation of the corneal bed is referred to in the section Adhesion Force Between the Short-Chain Hydrogel and Cornea. For the MSC-hydrogel group, 20  $\mu$ L of short-chain gellan gum solution with EdU-labeled Rb-BMSCs was dripped to the corneal stromal defect, and a bandage contact lens coated with  $\text{Ca}^{2+}$  was applied to cover the cornea. After 3 minutes, the contact lens was removed and the ocular surface was washed with PBS free of  $\text{Ca}^{2+}/\text{Mg}^{2+}$  for 3 times. For the hydrogel group, only short-chain gellan gum was used, whereas for the control group, no treatment was applied. Each group was given an 8-mg dose of tobramycin subconjunctival injection after surgery (Fig. 2).

### Imaging Study

Within 28 days after surgery, the anterior segment was photographed with a slit-lamp camera (Topcon Inc, Japan) to observe corneal stromal opacity that was graded as follows<sup>49</sup>: Grade 0, no corneal haze; Grade 1, iris details visible; Grade 2, pupillary margin visible, iris details not visible; Grade 3, pupillary margin not visible; and Grade 4, cornea totally opaque. A Scheimpflug system (Pentacam, OCULUS Inc, Germany) was used to detect corneal densitometry. Anterior segment optical coherence tomography (AS-OCT) (Casia2, TOMEY Inc, Japan) was used to determine material retention time, observe corneal stromal opacity and central corneal thickness (CCT), and calculate the central scar thickness ratio (percentage of central scar thickness to the CCT). The Fiji ImageJ 2.3.0 software was used to calculate stromal reflectivity and epithelial-stromal (E:S) reflectivity ratio based on AS-OCT parameters according to methods described by a previous study.<sup>48</sup>

### Hematoxylin and Eosin/Immunofluorescence Staining

Twenty-eight days after surgery, the rabbit eyeballs were enucleated and fixed with 4% paraformaldehyde (Solarbio, China) for 48 hours and washed twice with PBS. After being dehydrated in 30% sucrose solution (Macklin, China), the eyeballs were embedded in a optimal cutting temperature (O.C.T.) compound (Sakura, Japan) and sectioned to a thickness of 8 mm by a (Leica, Germany). Standard histologic techniques were performed for HE staining and immunofluorescence staining of cytokeratin 3 (CK3)/acetaldehyde dehydrogenase 3- $\alpha$ 1 (ALDH3A1)/ $\alpha$ -smooth muscle actin ( $\alpha$ -SMA). The click reaction solution was prepared according to the instructions of EdU labeling kit (Beyotime, China), and the sections of the MSC-hydrogel group were stained with the above solution to fluorescently trace EdU. The sections of the MSC-hydrogel group were stained with CK3,  $\alpha$ -SMA, and ALDH3A1 antibodies respectively and EdU fluorescence tracers, and different fluorescence channels were merged using Fiji ImageJ software.

### Gene Expression

RT-qPCR was performed on the 7th and 28th day postoperation and the target gene code for proteins participating in fibrosis of corneal stroma, including collagen type I- $\alpha$ 1 (COL1A1), collagen type V- $\alpha$ 1 (COL5A1), collagen type V- $\alpha$ 2 (COL5A2),  $\alpha$ -smooth muscle actin ( $\alpha$ -SMA), and vimentin (VIM). The primer design is shown in Supplemental Digital Content 2 (see Table, <http://links.lww.com/ICO/B624>).

### Western Blotting

To detect the expression level of  $\alpha$ -smooth muscle actin that is related to corneal fibrosis, on the 28th day postoperation, Western blotting was conducted and the main protocol was the same as mentioned in the section Western Blotting, except that the NC membrane was incubated with 1:1000  $\alpha$ -smooth muscle actin [1A4] mouse monoclonal antibody (Abcam).

### Statistical Analysis

Statistical analysis was performed by SPSS 20.0 software and diagramed by GraphPad Prism 9. The experimental data were expressed as mean  $\pm$  SD. The normal distribution and homogeneity of variance were first tested. The single-factor analysis of variance test was used to compare the mean of multiple samples. The independent sample *t* test was used to compare the mean of 2 groups. The difference was considered statistically significant when  $P < 0.05$ .

## RESULTS

### Characterization of Solutions and Hydrogels

#### Rheological Results of the Short-Chain and Native Gellan Gum Solution

The viscosity of the short-chain gellan gum solution decreased with the increase of incubation time (121°C, 0.1

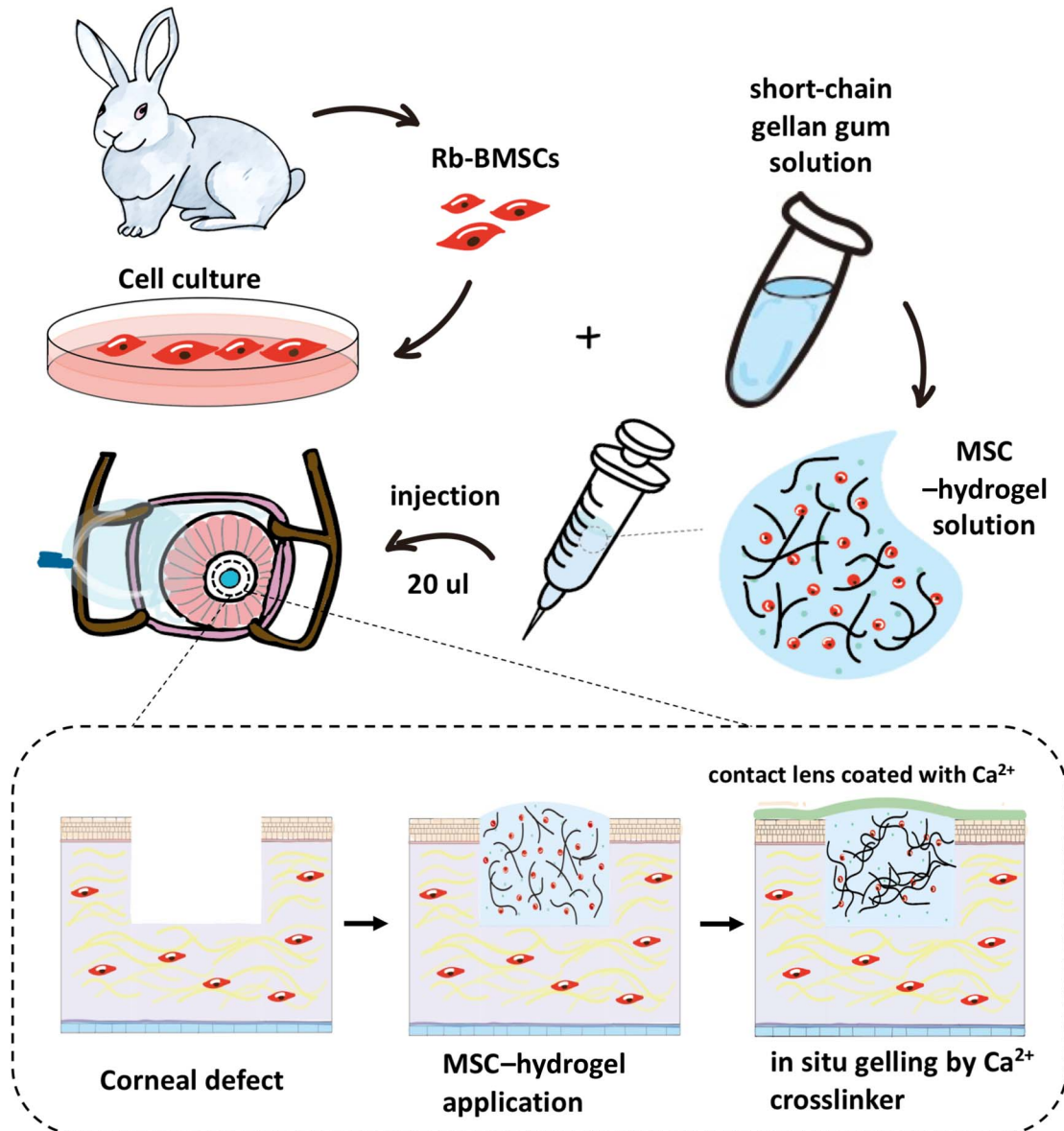


**FIGURE 2.** Overview of the operation. Primarily cultured Rb-BMSCs were mixed with 0.75% short-chain gellan gum solution under room temperature and applied to the corneal defect of the New Zealand white rabbit. In situ gelling happened when the mixture was covered by a bandage contact lens coated with  $\text{Ca}^{2+}$ .

MPa) and decreased sharply from 18 to 20 minutes and it reached below  $0.1 \text{ Pa}\cdot\text{s}$  (the criteria of low-viscosity liquid) from 20 minutes (Fig. 3A). From 10 to  $45^\circ\text{C}$ , the loss modulus of the short-chain gellan gum solution was larger than the storage modulus, indicating that there was no significant cross-linking in this temperature range (Fig. 3B). However, the loss modulus of the native gellan gum solution was smaller than the storage modulus, indicating significant cross-linking (Fig. 3B). In addition, with the increase of angular frequency (Fig. 3C) and oscillation strain (Fig. 3D), the phase angle of the short-chain gellan gum increased, indicating an increase of its viscosity and a decrease of its elasticity. The viscosity of short-chain gellan gum solution

decreased with the increase of shear rate and this “shear-thinning” characteristic (Fig. 3E) accorded with the rheological property of polymers. In addition, the viscosity of the short-chain gellan gum solution was lower than  $0.1 \text{ Pa}\cdot\text{s}$  at room temperature which made it a low-viscosity liquid, and no change was observed with the increase of testing time (Fig. 3F).

### Macroscopy and Scanning Electron Microscopy Observation

The native gellan gum solution stayed in gel form under room temperature, whereas the short-chain gellan gum solution stayed in liquid form under room temperature

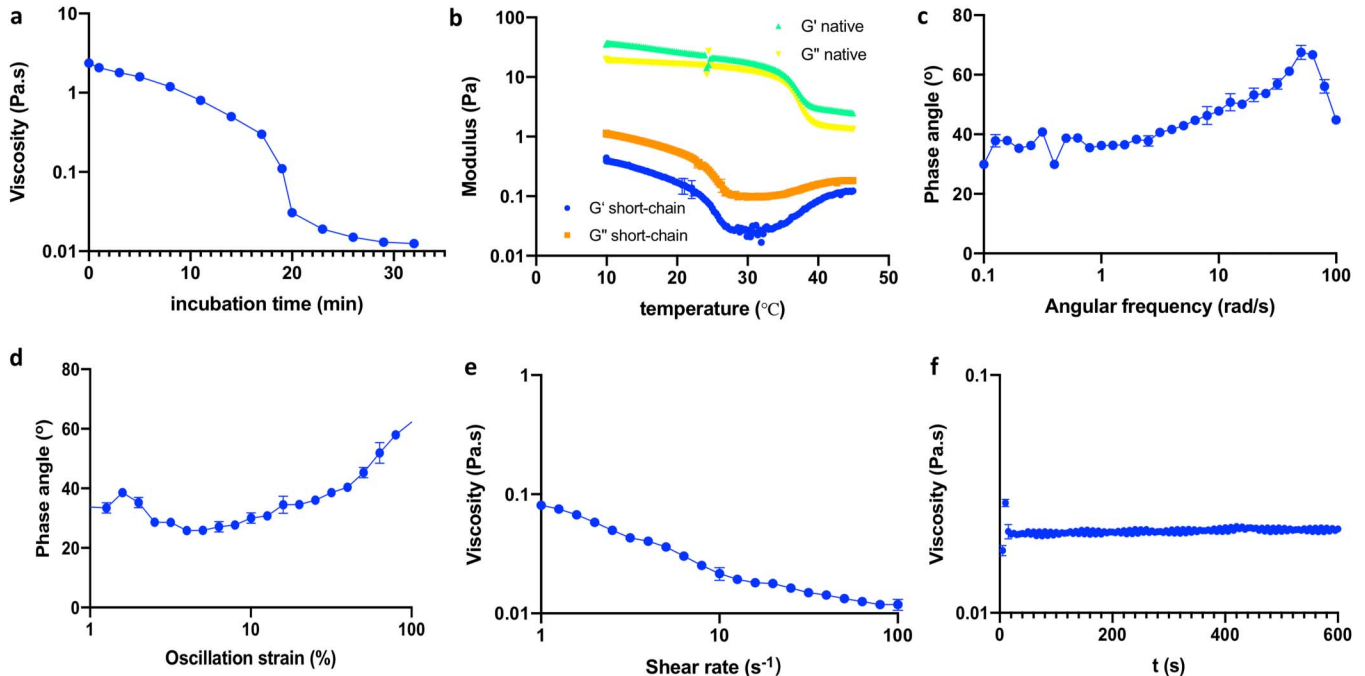


**FIGURE 3.** Rheological results of the short-chain and the native gellan gum solution. A, Viscosity of short-chain GG-G solution at different incubation times under high temperature and pressure. B, Temperature-dependent rheology of the short-chain and native gellan gum solution from 10 to 45°C. ( $G'$ : storage modulus and  $G''$ : loss modulus). C, Frequency-dependent rheology of the short-chain gellan gum solution at room temperature. D–F, Oscillatory strain-sweep tests, shear-dependent, and time-dependent viscosity changes of the short-chain gellan gum solution at room temperature.

(Fig. 4A). The short-chain gellan gum lyophilized for 72 hours formed a porous structure, and its overall morphology was more regular and uniform compared with the native gellan gum (Fig. 4B). Scanning electron microscopy showed that both native and short-chain gellan gum showed porous structures formed by ice crystal evaporation, whereas the latter had a smaller pore size of about 200 to 300  $\mu\text{m}$  and a more regular lamellar structure (Figs. 4C, D).

### Gel Permeation Chromatography Results

The peak molecular value of the native gellan gum was 5807.1 kD (Fig. 4E), whereas the value was 3092.4 kD for the short-chain gellan gum (Fig. 4F).

### Physical Properties

The light transmittance of the short-chain gellan gum was 89% to 92% in the visible region (Fig. 4G). The Young modulus of the short-chain gellan gum increased with the cross-linking time before it reached the plateau at 20 minutes. When crosslinked for 3 minutes, the Young modulus of the gel was  $(8.76 \pm 0.41)$  kPa, which was close to that of the rabbit corneal stroma (Fig. 4H). The in vitro dissolution rate of the short-chain gellan gum was  $(19.84 \pm 2.12)$  % on day 21 (Fig. 4I). The cell release rate of MSC-hydrogel was slowly increasing to  $(61.02 \pm 4.00)$  % on day 7 (Fig. 4J). The adhesion force between

the gel and the corneal bed was  $(0.07 \pm 0.02)$  N (Fig. 4K,  $n = 12$ ).

### Morphology and Molecular Phenotype of Rb-BMSCs

The extracted spindle-like MSCs (Fig. 5A) were successfully stained by an EdU tracer (Fig. 5B). In addition, the pluripotency of the extracted cells was validated by Oil Red O staining, Alizarin Red staining, and Alcian blue staining (Figs. 5C–E). The  $\text{CD34}^-/\text{CD29}^+$  phenotype of the extracted cells was proved by flow cytometry analysis and was accorded with that of MSCs (Figs. 5F, G).

### In Vitro Study

#### Optical Microscopy Observation of Rb-BMSC-Encapsulated Hydrogels

The cells were difficult to be evenly dispersed in the native gellan gum and many cell masses could be found (Fig. 6A). After 21 days of culture, most of the cells showed no significant change (Fig. 6B). For the short-chain gellan gum, the cells were uniformly dispersed in a single-cell state (Fig. 6C). The cells gradually extended into spindle-like cells when cultured to 21 days (Fig. 6D). The cell masses counted per field of view ( $10 \times 10$ ) on the first day were  $685.0 \pm 65.2$  for the short-chain gellan gum group and  $201.3 \pm 28.7$  for the native gellan gum group ( $n = 4$ ,  $P < 0.0001$ ) (Fig. 6E).

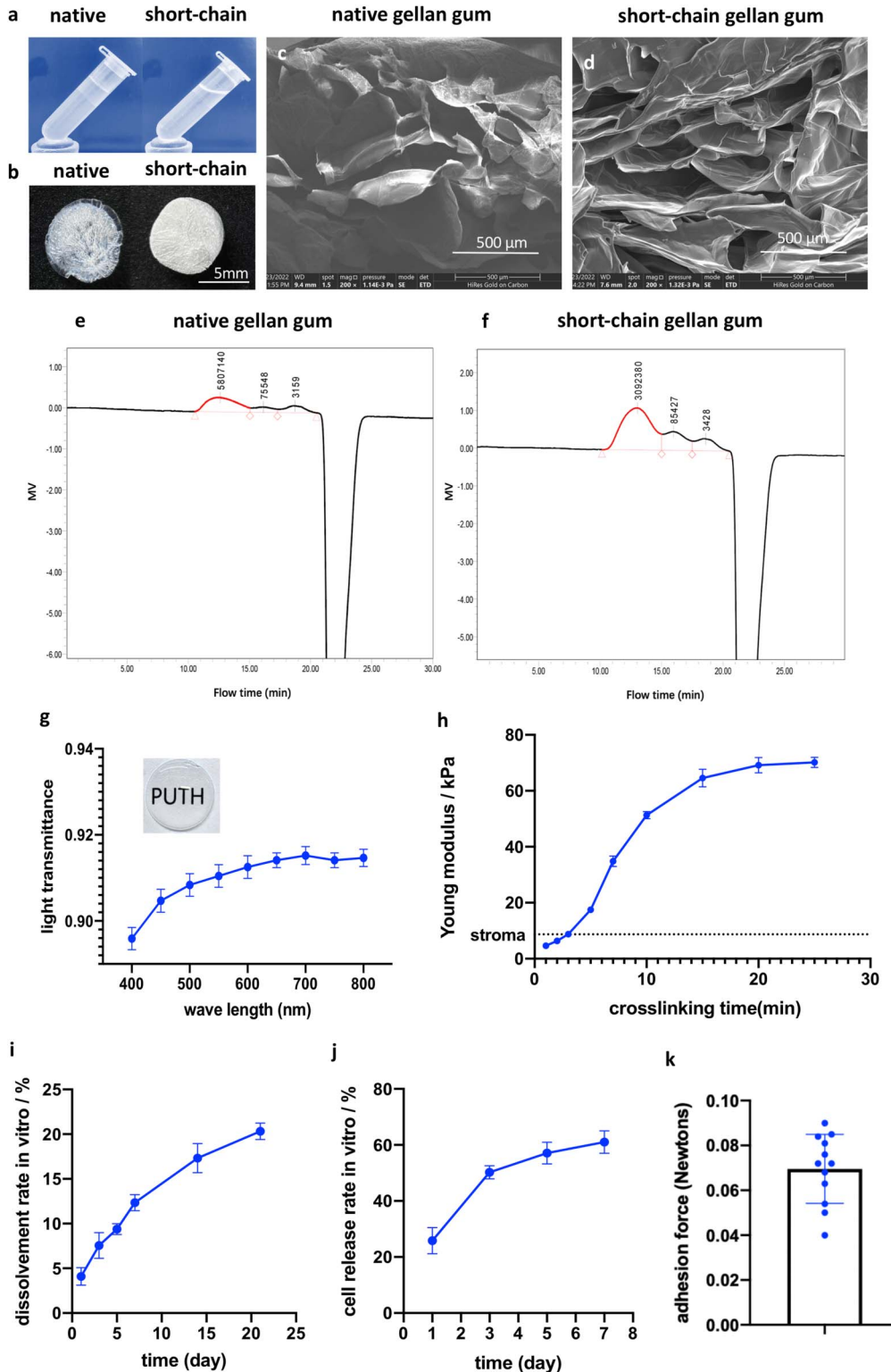


**FIGURE 4.** 0.75% native gellan gum solution (A, left) and 0.75% short-chain gellan gum solution (A, right) at room temperature; Macroscopy of the lyophilized native gellan gum (B, left) and short-chain gellan gum (B, right). Scanning electron microscopy of the native gellan gum (C) and short-chain gellan gum (D). Gel permeation chromatography of native gellan gum (E) and short-chain gellan gum (F). The peak molecular value (Mp) was calculated and marked on the curve. G–I, Light transmittance, Young’s modulus and dissolvment rate of the short-chain gellan gum. J, Cell release rate of MSC–hydrogel. K, Adhesion force between the hydrogel and the corneal defect (n = 12).

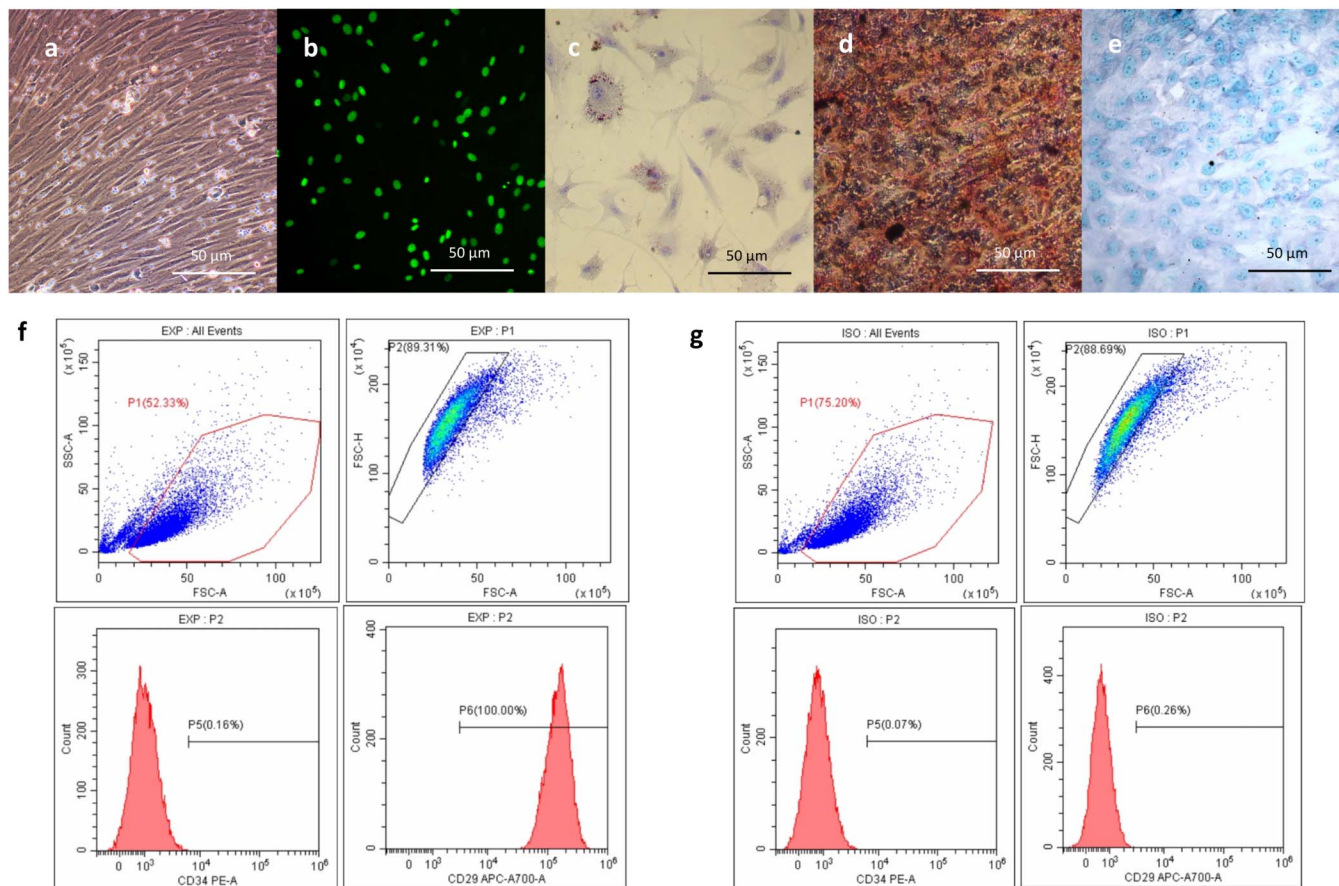


**FIGURE 5.** A, Rb-BMSCs of primary culture. B, EdU labeling of nuclei of Rb-BMSCs. C–E, The adipogenic, osteogenic, and chondrogenic differentiation of BMSCs was detected by Oil Red O, Alizarin Red S, and Alcian blue staining, respectively. Flow cytometry of CD34 and CD29 of the experimental group (F) and the isotype control group (G).

### Cell Viability and Toxicity Assay

Cell viability and toxicity assay plays an irreplaceable role in testing the biocompatibility of tissue-engineered materials. Live/dead cell staining found that the living cell percentage in the short-chain gellan gum was more than 90% on the 7th, 14th, and 21st day, whereas in the native gellan gum, it was  $(73 \pm 3.2)\%$  on day 7,  $(70 \pm 4.5)\%$  on day 14, and  $(55 \pm 4.9)\%$  on day 21 ( $n = 4$ ,  $P < 0.0001$ ) (Figs. 6F, G). CCK8 assay showed that within 21 days, the activity of cells cultured in the short-chain gellan gum was higher than that of the native gellan gum ( $n = 4$ ,  $P < 0.0001$ ) (Fig. 6H).

### RT-qPCR and Western Blotting

After being cultured in the short-chain gellan gum for 21 days, the relative expression of mRNA coding for DCN, lumican (LUM), and KERA increased by 127.8-fold, 165.5-fold, and 25.4-fold, respectively ( $n = 3$ ,  $P < 0.05$ ), whereas there was no significant difference in the expression of the other detected genes ( $P > 0.05$ ) (Fig. 7A). Western blotting results confirmed the qPCR results showing that DCN, lumican, and KERA were upregulated at the protein level (Fig. 7B).

### In Vivo Study

#### Imaging Study

On the operation day, the MSC-hydrogel and the pure hydrogel were both embedded smoothly and uniformly in the corneal stromal defect (Fig. 8A, row 1). Two days post-operation, the defects of the corneal stroma were still filled with regular hydrogels (Fig. 8A, row 2). On the fifth day postoperation, the volume of the hydrogels decreased and the shapes were irregular (Fig. 8A, row 3). For both of the groups, from the seventh day postoperation, the hydrogels were not detected and the corneal defects were covered by continuous epitheliums (Figs. 9A, B). The material retention time was  $(5.25 \pm 0.87)$  days and  $(5.17 \pm 0.58)$  days for the hydrogel group and the MSC-hydrogel group, respectively ( $n = 12$ ,  $P > 0.05$ ) (Fig. 8B).

Corneal nebula or macula appeared in the 3 groups from the seventh day postoperation. However, the degree of central corneal opacity in the MSC-hydrogel group was lower, which was mainly the nebula, whereas it was the macula for the other 2 groups (Fig. 9A). The central cornea with a high reflection rate shown in AS-OCT represented

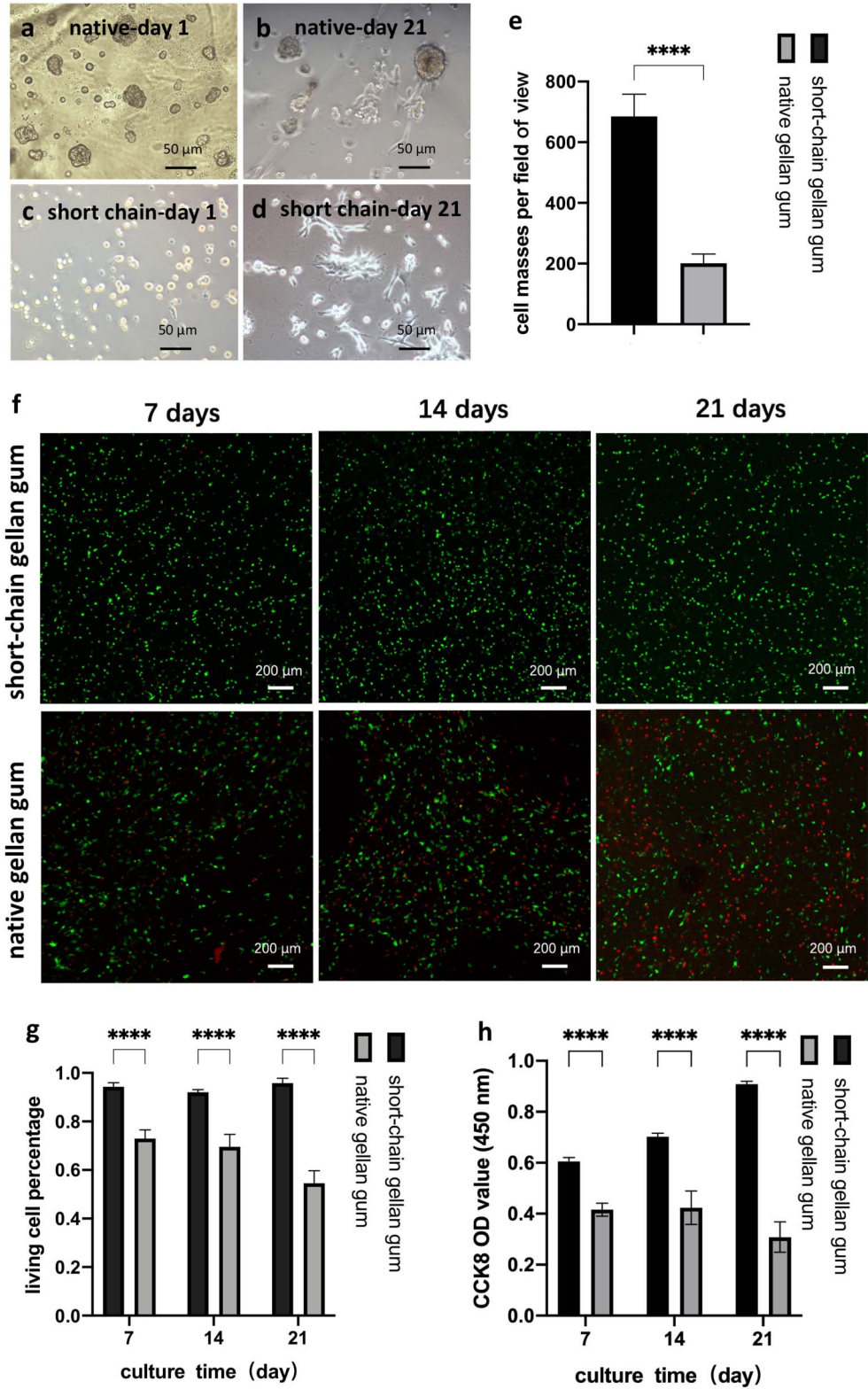


**FIGURE 6.** A, Cells mixed with the native gellan gum at 39°C. B, Cells encapsulated in the native gellan gum on day 21. C, Cells mixed with the short-chain gellan gum under room temperature. D, Cells encapsulated in the short-chain gellan gum on day 21. E, Cell masses counted per 10 × 10 field. F, Calcein AM/PI live (green) and dead (red) staining. About 900 cells per sample were counted for percentage values. G, Living cell percentage of live/dead staining. H, CCK8 assay (\**P* < 0.05, \*\**P* < 0.01, \*\*\**P* < 0.001, s\*\*\*\**P* < 0.0001).

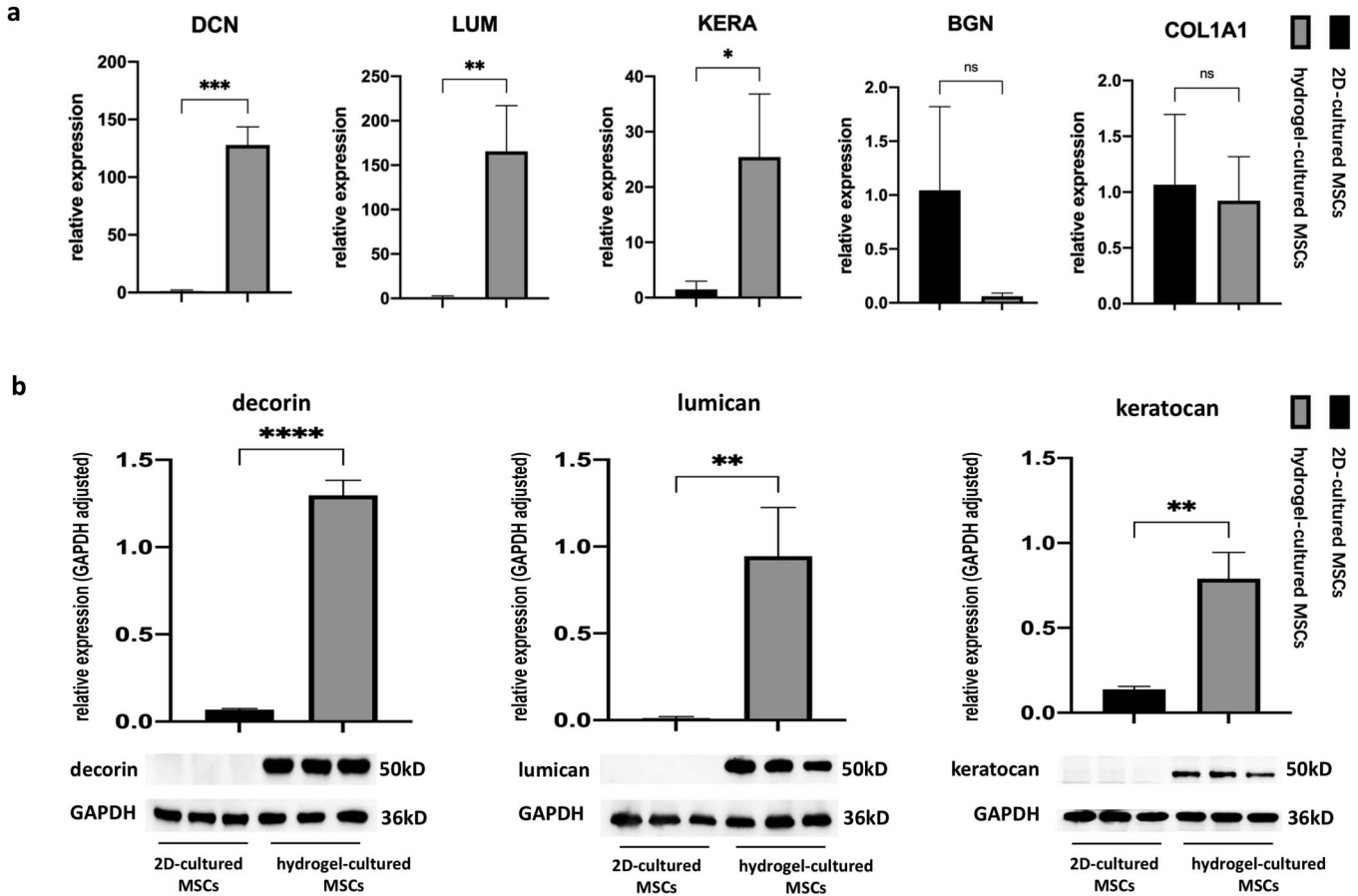


**FIGURE 7.** RT-qPCR (A) and western blotting results (B) of Rb-BMSCs cultured in the short-chain gellan gum for 21 days (\* $P < 0.05$ , \*\* $P < 0.01$ , \*\*\* $P < 0.001$ , \*\*\*\* $P < 0.0001$ ).

a corneal scar (Fig. 9B), and the differences between groups agreed with the results of the anterior segment photography.

From Figure 9C, we can see that, on day 28 postoperation, the corneal haze grade of the MSC-hydrogel group was significantly lower ( $n = 4$ ,  $P < 0.0001$ ). The MSC-hydrogel group had a smaller CCT ( $n = 4$ ,  $P < 0.05$ ) with a lower central corneal scar thickness ratio ( $n = 4$ ,  $P < 0.001$ ). The stromal reflectivity was lower in the MSC-hydrogel group ( $n = 4$ ,  $P < 0.05$ ) while its E:S reflectivity ratio was higher ( $n = 4$ ,  $P < 0.0001$ ). The corneal densitometry of the MSC-hydrogel group was  $(20.73 \pm 1.85)$  Grayscale units which was lower than that of the other 2 groups ( $n = 4$ ,  $P < 0.05$ ).

**HE/Immunofluorescence Staining**

HE staining (Fig. 10A) showed that for the MSC-hydrogel group, the corneal stromal staining was more homogeneous with cells evenly distributed in the stroma, whereas for the other 2 groups, excessive cells gathered irregularly in the upper stroma with more eosinophilic staining of the ECM. Moreover, for the control group, the newborn corneal epithelium was thickened. HE staining for all 3 groups is given in Supplemental Digital Content 3 (see Figure, <http://links.lww.com/ICO/B623>).

The immunofluorescence staining using  $\alpha$ -SMA antibodies was designed to show the distribution of myofibroblasts (Fig. 10B). The normal cornea showed no positive fluorescence signals, whereas a small amount of red fluorescence signals could be seen on the interface between corneal epithelium and stroma in the MSC-hydrogel group. For the hydrogel group and control group, a large amount of red fluorescence signals could be detected in the upper layers of the central corneal stroma (Fig. 10B). Results showed that CK3-labeled corneal epithelial cells and  $\alpha$ -SMA-labeled myofibroblasts did not overlap with EdU-labeled MSC-derived cells, suggesting that the transplanted MSCs did not differentiate to corneal epithelial cells or myofibroblasts (Figs. 10C, D). However, the differentiation of MSCs to keratocytes was demonstrated by the colocalization of EdU and keratocyte marker ALDH3A1, as shown in Figure 10E, where among native keratocytes expressing ALDH3A1 in the cytoplasm (red), the differentiated keratocytes from MSCs somewhat occurred with their cytoplasm stained red (ALDH3A1) and nucleus stained green (EdU). However, considering the large number of implanted MSCs (with the nucleus stained green), the percentage of their differentiation to keratocytes was relatively small.

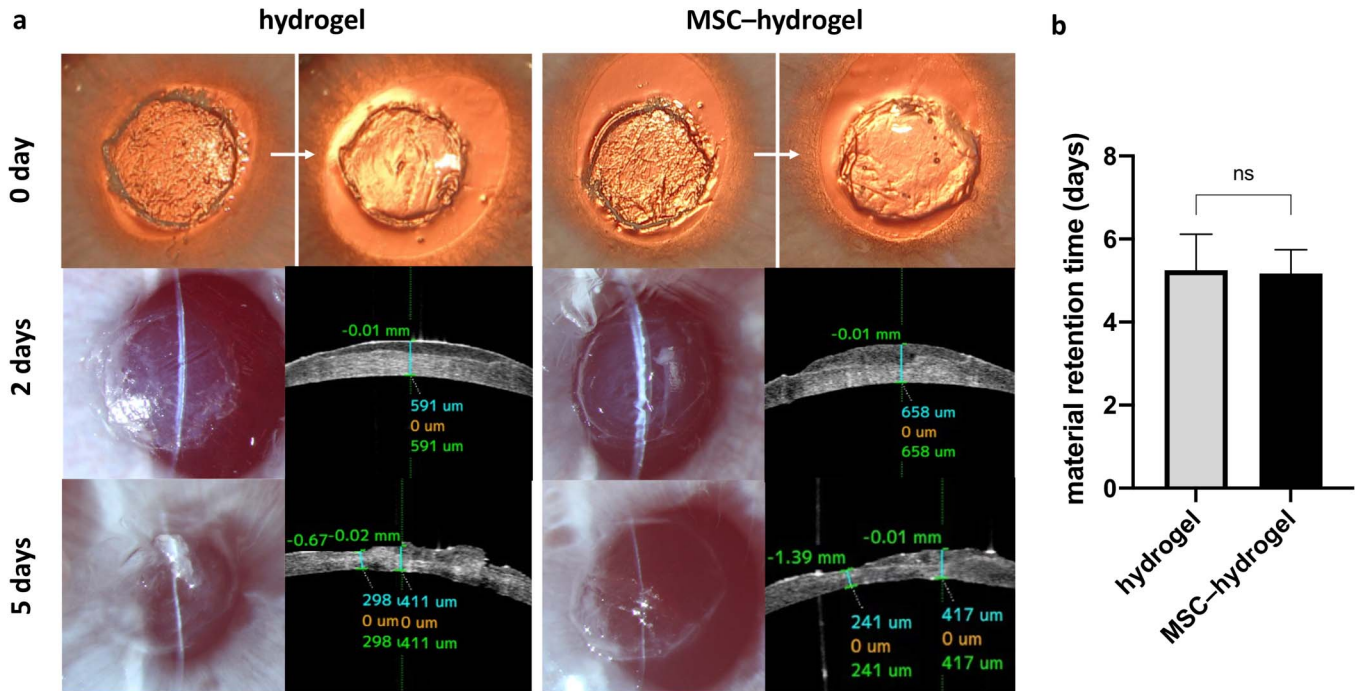


**FIGURE 8.** A, row 1, Anterior lamellar keratotomy of the central cornea on the operation day and in situ gelling of hydrogels. A, row 2, Two days postop, transparent light bands could be seen in front of the corneal stroma defect which represented the hydrogel/MSChydrogel. A, row 3, Five days postop, the transparent light bands became irregular and even missing in certain areas. B, Material retention time between groups. (\* $P < 0.05$ , \*\* $P < 0.01$ , \*\*\* $P < 0.001$ , \*\*\*\* $P < 0.0001$ ).

### RT-qPCR and Western Blotting

RT-qPCR results showed that the relative expression of mRNA coding for  $\alpha$ -smooth muscle actin ( $\alpha$ -SMA), vimentin (VIM), collagen type 5- $\alpha$ 1 (COL5A1), and collagen type 1- $\alpha$ 1 (COL1A1) of the MSC-hydrogel group was lower than the other 2 groups 7 days postoperation ( $n = 3$ ,  $P < 0.01$ ), and there was no significant difference between the latter 2 groups ( $n = 3$ ,  $P > 0.05$ ). On day 28 postoperation, the relative expressions of mRNA coding for  $\alpha$ -SMA and COL5A1 of the MSC-hydrogel group was lower than the other 2 groups ( $n = 3$ ,  $P < 0.01$ ), still there was no significant difference between the latter 2 groups ( $n = 3$ ,  $P > 0.05$ ) (Fig. 11A). Western blotting results showed that on the 28th day postoperation, the expression level of  $\alpha$ -smooth muscle actin in the MSC-hydrogel group was lower than that of the hydrogel group and the control group ( $n = 3$ ,  $P < 0.0001$ ), and no significant difference was found between the latter 2 groups ( $n = 3$ ,  $P > 0.05$ ) (Fig. 11B).

### DISCUSSION

The aim of this research was to find a material that can stay on the ocular surface for a long time and slowly release MSCs. This material needs to meet the following requirements: First, it should be a low-viscosity liquid under room temperature, so that it can be evenly mixed with MSCs. Second, this material should be biocompatible, which means it should be neither toxic to MSCs nor aggravating the opacity of the corneal stroma.

Furthermore, this material needs to stay on the ocular surface for enough time to slowly release MSCs for satisfactory therapeutic outcomes. Last but not the least, this material should be transparent to preserve the visual acuity of the patient during treatment. Among tissue-engineered materials, gellan gum meets most of the above requirements. It is a linear anionic polymer composed of 4 monosaccharide units (1,3- $\beta$ -D-glucose, two 1,4- $\beta$ -D-glucose, and 1,4- $\alpha$ -L-rhamnose). Its long-chain molecular structure is formed by the above repeated units to reach a relative molecular weight of about 500 kD.<sup>34</sup> Gellan gum is favored by biomedical research, but native gellan gum has a fatal disadvantage that its gelling temperature is as high as 50°C.<sup>50</sup> At this temperature, cells are prone to thermal damage and thus limits its application for constructing cell-encapsulating scaffolds. According to previous studies, the weight/volume of gellan gum should be at least 0.5% to form a hydrogel stable enough for tissue engineering. However, even if the concentration of native gellan gum is reduced to 0.5%, according to rheological analyses,  $G' > G''$  still exists,<sup>51</sup> indicating that the hydrogel is still crosslinked. As a result, its viscosity is greater than 0.1 Pa·s,<sup>52</sup> which excludes it from being a low-viscosity liquid. To lower its gelling temperature, Chen et al<sup>53</sup> modified native gellan gum by adding methacrylic anhydride, but the operation process was quite complicated. In this study, we offered a simple and effective method to modify native gellan gum by high temperature and pressure (121°C and 0.1 MPa for 20 minutes), so that it stays in liquid form under room temperature. We speculated that this was related to shorter molecular chains of the

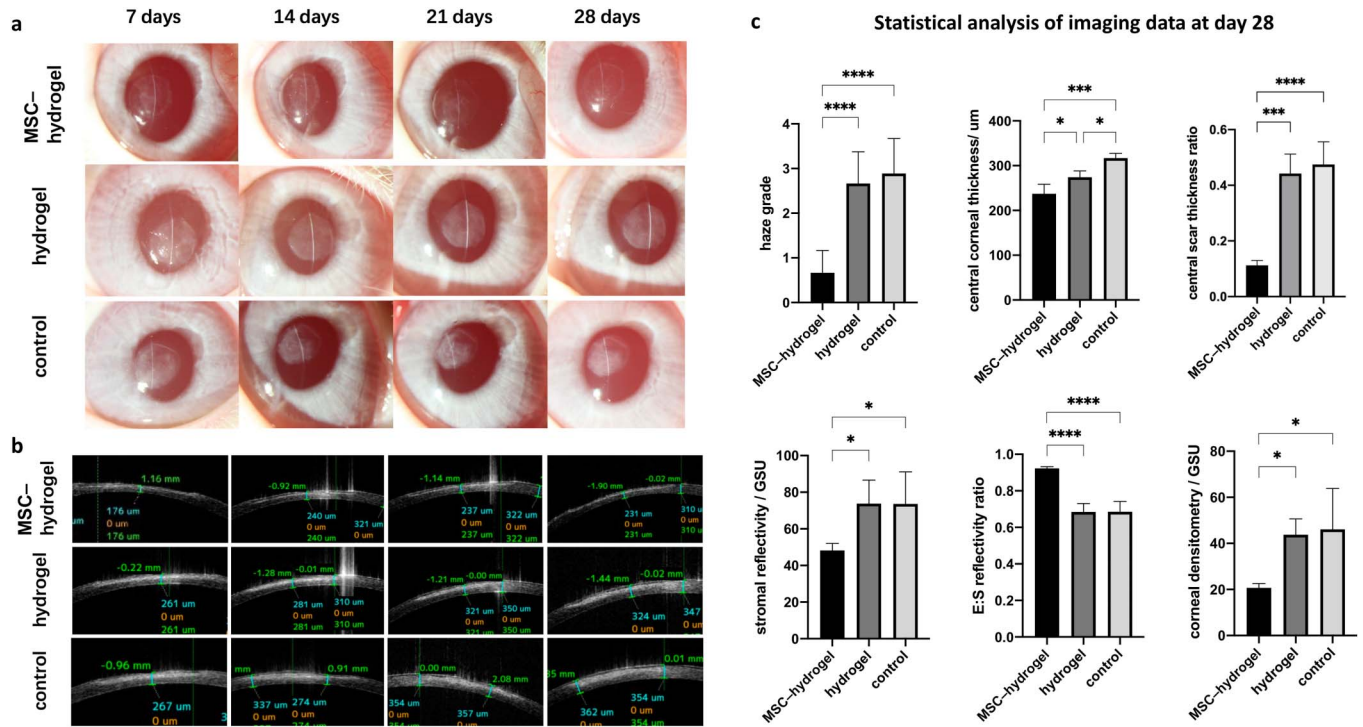


**FIGURE 9.** A, Anterior segment photography. B, AS-OCT. C, Statistical analysis of the imaging data at day 28. (\* $P < 0.05$ , \*\* $P < 0.01$ , \*\*\* $P < 0.001$ , \*\*\*\* $P < 0.0001$ ).

modified gellan gum according to gel permeation chromatographic results. We settled on 121°C and 0.1 MPa because this recipe coordinates with the high-temperature and high-pressure disinfection procedure which is available at almost all hospitals. The reason for setting 20 minutes is because we found, as shown in Figure 3A, that the curve of viscosity drops sharply from 18 to 20 minutes and it reaches below 0.1 Pa·s (the criteria of low-viscosity liquid) just at 20 minutes. A shorter incubation time will lead to a higher viscosity (Fig. 3A) of the gel solution at room temperature, which is not suitable for mixing cells evenly, whereas a longer incubation time will increase the  $\text{Ca}^{2+}$  cross-linking time, which is unnecessary and uneconomical. Moreover, this recipe is a physical method that does not introduce other substances that may be potentially toxic to the encapsulated cells. Rheological results showed that the short-chain GG-G solution we prepared had stable fluid characteristics under room temperature, and its viscosity was lower than 0.1 Pa·s, which made it a low-viscosity fluid.<sup>54</sup> However, compared with the native gellan gum that was highly crosslinked at room temperature by forming double-strand helices, the short-chain GG-G solution was more suitable to mix cells with lower viscosity. In previous studies, to mix cells evenly with native gellan gum, the temperature of the system was often elevated to 40 to 45°C to acquire lower viscosity of the gel.<sup>55–57</sup> However, according to our findings, when mixing MSCs with native gellan gum at 39°C, irreversible thermal damage happened to the cells, resulting in immediate deaths of some cells and apoptosis of the others. As a result, the proportion of dead cells after 7 days of cell culture was as high as 48.6%. Moreover, large amounts of cell masses in the native gellan gum may be

caused by the rapid cooling and condensation of the gel solution in the process of cell mixing. However, cells can be dispersed more evenly in the short-chain gellan gum solution under room temperature with a lower ratio of cell death (<10%). However, it can be seen in this study that the short-chain gellan gum with lower gelling temperature had incomparable advantages in encapsulating cells over the native gellan gum.

The transparency, cell release rate, and adhesion to the cornea of the hydrogel are also important parameters for this study. The hydrogel will be used on the corneal surface, so its high transparency protects visual functions. The light transmittance in the visible region of the short-chain gellan gum represents the transparency of the material and was as high as 89% to 92%, which is close to that of the human corneal stroma.<sup>58,59</sup> Moreover, we hope that the hydrogel can stay on the ocular surface for enough time and degrade slowly, so that Rb-BMSCs can be released slowly onto the ocular surface to acquire satisfactory therapeutic outcomes. The in vitro cell release rate of the short-chain gellan gum was  $(61.02 \pm 4.00)\%$  on day 7 which was quite satisfactory. For adhesion of the gel to the cornea, the adhesion force was  $(0.07 \pm 0.02)$  N and was close to that between the laser in situ keratomileusis-like flaps and corneal bed.<sup>44</sup> Moreover, we observed that on the fifth day postoperation, some residual hydrogels could still be seen from the slitlamp and AS-OCT, which confirmed that the short-chain gellan gum had sufficient adhesion to the corneal stromal defect.

As to the regulations of materials for MSCs' gene expressions, we found that after being cultured in the short-chain gellan gum for 21 days, the expression of mRNAs

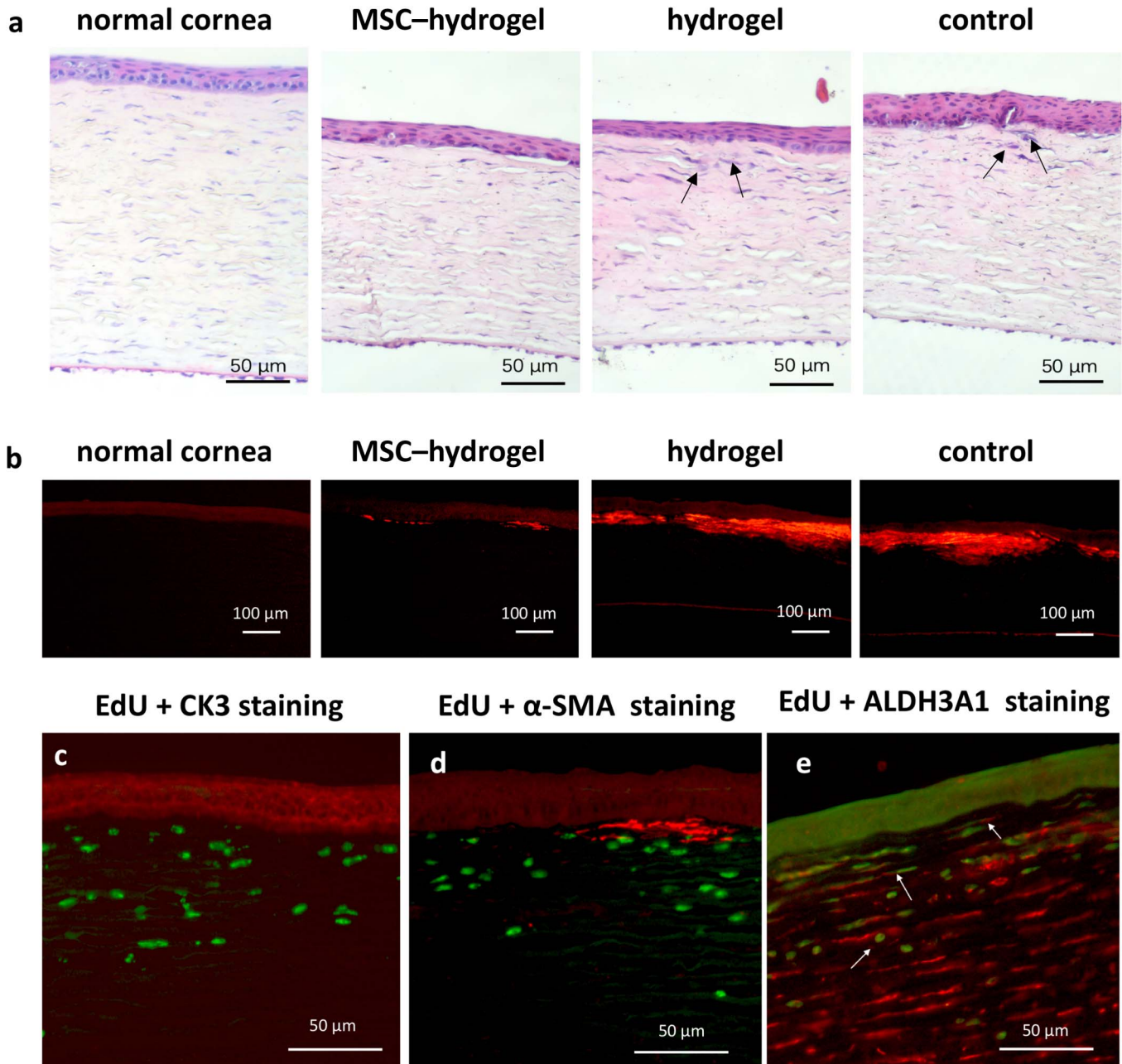


**FIGURE 10.** A, HE staining of the normal rabbit cornea and experimental samples on the 28th day postop. Black arrow heads indicate excessive cells gathered irregularly in the upper corneal stroma with more eosinophilic staining of the ECM. B, Immunofluorescence staining of  $\alpha$ -SMA to show the distribution of myofibroblasts. Samples of the MSC–hydrogel group were stained with CK3 (C),  $\alpha$ -SMA (D), ALDH3A1 (E) antibodies (red) and EdU fluorescence tracers (green).

coding for DCN, lumican, and KERA increased by 127.8-fold, 165.5-fold, and 25.4-fold, respectively ( $P < 0.05$ ), and was verified by Western blotting results. To the best of our knowledge, this finding is meaningful because it implies 3D-cultured MSCs' differentiation to keratocytes. As we know, the corneal stroma is mainly composed of keratocytes, type I collagen, type V collagen, and small leucine-rich proteogly-

can family (SLRP family) including DCN, lumican, KERA, and biglycan.<sup>47</sup> The SLRP family is not only the basis of corneal transparency but also functional markers of keratocytes.<sup>60,61</sup> As a result, the upregulated genes of DCN, LUM, and KERA in this study serve as the evidences of MSCs' differentiation to keratocytes. The mechanisms of this differentiation are suspected as follows: First, the Young

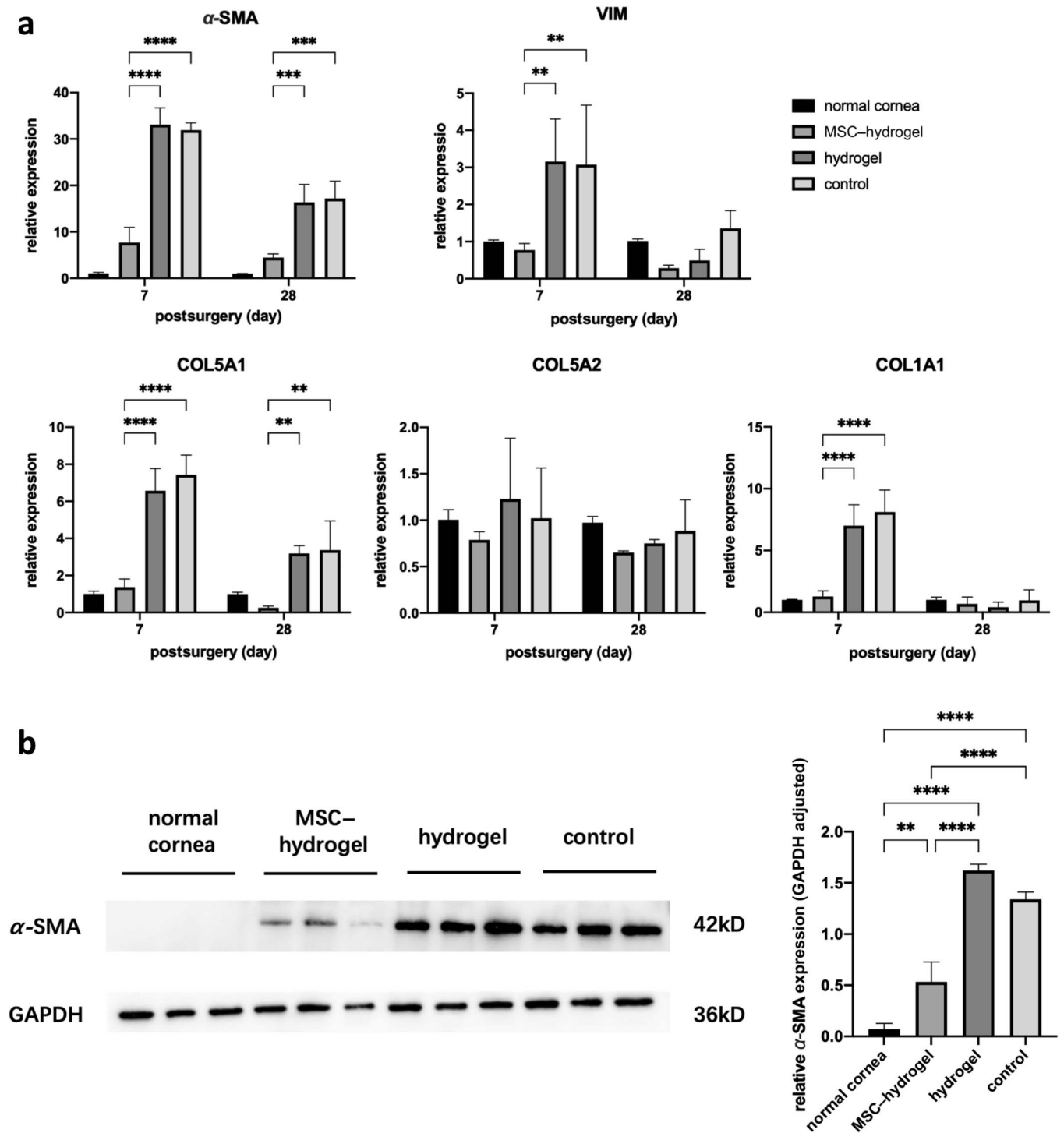


**FIGURE 11.** A, RT-qPCR results of the 3 groups 7 days and 28 days postoperation. B, western blotting results of the above 3 groups and the normal cornea.

modulus of the short-chain gellan gum was close to the corneal stroma and was critical for MSCs' differentiation, which was supported by the findings of Liu et al<sup>62</sup> that the differentiation of the encapsulated MSCs was dependent on hydrogel stiffness. Second, the microenvironment abundant

with glycosidic bonds provided by the short-chain gellan gum was also very important because it mimicked the microenvironment of the corneal stroma where the SLRP family members are also characterized by abundant glycosidic bonds. In previous studies, the traditional methods of

inducing MSCs to differentiate into keratocytes can be classified as coculture in the presence of keratocytes<sup>63</sup> and cultivation in specialized keratocyte growth media.<sup>20,64</sup> Recently, there are new induction methods emerging, such as mechanical stress method.<sup>65</sup> Among all induction methods, simulating the microenvironment of the corneal stroma is the key to success.<sup>66</sup> From the view of material science, surveys of MSCs' differentiation into terminal cells induced by biomaterials or synthetic materials are increasing nowadays, of which the induction into chondrocytes is the hotspot.<sup>55,67</sup> In our study, biomaterials are used to simulate the microenvironment of corneal stroma and its potential of promoting differentiation of MSCs to keratocytes was recognized.

For the choice of animal model to create corneal stromal opacity, we once tried the classical chemical injury model.<sup>9</sup> Although it did produce significant corneal opacification, it was too severe and tended to cause more uncontrollable complications, such as symblepharon, iritis, and synechiae, which made the data analysis troublesome. After extensive literature search, we finally chose the rabbit model of anterior lamellar keratectomy.<sup>48</sup> The study by Chandru et al<sup>31</sup> used the above model to evaluate the therapeutic effects of human cornea-derived decellularized ECM as an accessible therapeutic alternative for corneal anterior stromal reconstruction and achieved positive outcomes. In addition, Zhao et al<sup>68</sup> used a similar animal model to confirm the effectiveness of a collagen-based material combined with microRNA for inhibiting corneal scar formation. Together with our study, this rabbit model of anterior lamellar keratectomy proves to be reliable and valid in creating moderate corneal stromal opacity.

Compared with the hydrogel group and control group, the rabbit corneal defect treated with MSC-hydrogel was more transparent on the 28th day after operation, showing lower central corneal scar ratio, lower densitometry value, lower stromal reflectivity, and higher E:S reflectivity ratio. In addition, in the MSC-hydrogel group, the fibrosis marker  $\alpha$ -SMA was less detected in fluorescence staining and its gene and protein expressions were downregulated compared with the other 2 groups. However, there were no significant differences of the above parameters between the hydrogel group and control group. It indicated that the short-chain gellan gum itself will not aggravate corneal opacity while the preventive effect of MSC-hydrogels for corneal stromal opacity was achieved exactly by the MSCs encapsulated in the hydrogel. Moreover, we also found that on the 28th day postoperation, the implanted Rb-BMSCs invaded the upper corneal stroma and some of them expressed ALDH3A1, a specific marker of keratocytes, which confirmed their differentiation into keratocytes.

The major limitation of our study is that no increase of the CCT was observed in the MSC-hydrogel group at the end of the research. We think it is because first, the implanted MSC-hydrogel stays in place just long enough for the cornea to reepithelialize without scarring. However, this period is still inadequate for providing sustained delivery of MSCs or MSC-derived keratocytes to promote corneal stromal regeneration. Second, once the corneal epithelial wound is closed, there would be no further signals to direct the keratocytes to

produce excessive amounts of collagen. Instead a homeostasis is achieved after epithelial closure, such that the new thickness of the cornea would be maintained and not increasing over time. Therefore, it would be much more beneficial if this biomaterial could stay in the cornea for a longer time to delay epithelial closure and gain a larger window for MSC-derived keratocytes to promote corneal stromal regeneration. Considering the fact that although the defective cornea was relatively transparent in the MSC-hydrogel group, its thickness was not restored. It reminds us that this treatment with MSC-hydrogel should be forbidden when corneal stromal defects are close to forming corneal perforations because in those situations, mechanical strength provided by scars would be more important than corneal transparency. Another shortfall of this study is that an additional group with only MSCs would have been preferable to acquire a more precise conclusion. However, based on previously published researches, only a few have used the above group because of its low efficiency.<sup>7,69</sup> Moreover, according to a recently published review summarizing different strategies for topical use of MSCs to treat ocular surface disease, it pointed out that for MSC therapy to be efficacious, a cell-carrying scaffold is required to prevent MSCs from being expelled through lachrymation and blinking.<sup>70</sup>

In conclusion, this type of short-chain gellan gum encapsulates Rb-BMSCs through in situ cross-linking, allowing MSCs to slowly release to the corneal stromal defect and prevent corneal stromal opacity. Furthermore, some of the implanted Rb-BMSCs can integrate into the upper corneal stroma and differentiate into keratocytes in vivo.

## REFERENCES

1. Ljubimov AV, Saghizadeh M. Progress in corneal wound healing. *Prog Retin Eye Res.* 2015;49:17–45.
2. Pascolini D, Mariotti SP. Global estimates of visual impairment: 2010. *Br J Ophthalmol.* 2012;96:614–618.
3. Wong KH, Kam KW, Chen LJ, et al. Corneal blindness and current major treatment concern-graft scarcity. *Int J Ophthalmol.* 2017;10:1154–1162.
4. Flaxman SR, Bourne RRA, Resnikoff S, et al. Global causes of blindness and distance vision impairment 1990–2020: a systematic review and meta-analysis. *Lancet Glob Health.* 2017;5:e1221–e1234.
5. Gain P, Jullienne R, He Z, et al. Global survey of corneal transplantation and eye banking. *JAMA Ophthalmol.* 2016;134:167–173.
6. Mohan RR, Kempuraj D, D'Souza S, et al. Corneal stromal repair and regeneration. *Prog Retin Eye Res.* 2022;91:101090.
7. Almalotit D, Koliakos G, Papakonstantinou E, et al. Mesenchymal stem cells improve healing of the cornea after alkali injury. *Graefes Arch Clin Exp Ophthalmol.* 2015;253:1121–1135.
8. Call M, Elzarka M, Kunesh M, et al. Therapeutic efficacy of mesenchymal stem cells for the treatment of congenital and acquired corneal opacity. *Mol Vis.* 2019;25:415–426.
9. Sharma J, Sharma RK, Gupta P, et al. Corneal reconstruction in chemically damaged cornea using temperature responsive surface assisted mesenchymal stem cell transplantation in rabbits. *Graefes Arch Clin Exp Ophthalmol.* 2021;259:1859–1870.
10. Yun YI, Park SY, Lee HJ, et al. Comparison of the anti-inflammatory effects of induced pluripotent stem cell-derived and bone marrow-derived mesenchymal stromal cells in a murine model of corneal injury. *Cytotherapy.* 2017;19:28–35.
11. Ghannam S, Bouffi C, Djouad F, et al. Immunosuppression by mesenchymal stem cells: mechanisms and clinical applications. *Stem Cell Res Ther.* 2010;1:2.

12. Omoto M, Katikireddy KR, Rezazadeh A, et al. Mesenchymal stem cells home to inflamed ocular surface and suppress allosensitization in corneal transplantation. *Invest Ophthalmol Vis Sci.* 2014;55:6631–6638.
13. Orozco Morales ML, Marsit NM, McIntosh OD, et al. Anti-inflammatory potential of human corneal stroma-derived stem cells determined by a novel in vitro corneal epithelial injury model. *World J Stem Cells.* 2019;11:84–99.
14. Sherman AB, Gilger BC, Berglund AK, et al. Effect of bone marrow-derived mesenchymal stem cells and stem cell supernatant on equine corneal wound healing in vitro. *Stem Cell Res Ther.* 2017;8:120.
15. Xu G, Zhang L, Ren G, et al. Immunosuppressive properties of cloned bone marrow mesenchymal stem cells. *Cell Res.* 2007;17:240–248.
16. Tang Q, Lu B, He J, et al. Exosomes-loaded thermosensitive hydrogels for corneal epithelium and stroma regeneration. *Biomaterials.* 2022;280:121320.
17. Demirayak B, Yüksel N, Çelik OS, et al. Effect of bone marrow and adipose tissue-derived mesenchymal stem cells on the natural course of corneal scarring after penetrating injury. *Exp Eye Res.* 2016;151:227–235.
18. Mittal SK, Omoto M, Amouzegar A, et al. Restoration of corneal transparency by mesenchymal stem cells. *Stem Cell Rep.* 2016;7:583–590.
19. Espandar L, Bunnell B, Wang GY, et al. Adipose-derived stem cells on hyaluronic acid-derived scaffold: a new horizon in bioengineered cornea. *Arch Ophthalmol.* 2012;130:202–208.
20. Du Y, Roh DS, Funderburgh ML, et al. Adipose-derived stem cells differentiate to keratocytes in vitro. *Mol Vis.* 2010;16:2680–2689.
21. Liu H, Zhang J, Liu CY, et al. Bone marrow mesenchymal stem cells can differentiate and assume corneal keratocyte phenotype. *J Cell Mol Med.* 2012;16:1114–1124.
22. Liu H, Zhang J, Liu CY, et al. Cell therapy of congenital corneal diseases with umbilical mesenchymal stem cells: lumican null mice. *PLoS One.* 2010;5:e10707.
23. Mooney DJ, Vandenburgh H. Cell delivery mechanisms for tissue repair. *Cell Stem Cell.* 2008;2:205–213.
24. Bafna RK, Tripathi M, Asif MI, et al. Management of small perforated corneal ulcers: training model in mammalian eye to enhance surgical skills of residents. *Eur J Ophthalmol.* 2021;25:11206721211035628.
25. Chun YH, Park SK, Kim EJ, et al. In vivo biocompatibility evaluation of in situ-forming polyethylene glycol-collagen hydrogels in corneal defects. *Sci Rep.* 2021;11:23913.
26. Chen F, Mundy DC, Le P, et al. In situ-forming collagen-hyaluronate semi-interpenetrating network hydrogel enhances corneal defect repair. *Transl Vis Sci Technol.* 2022;11:22.
27. Chen F, Le P, Fernandes-Cunha GM, et al. Bio-orthogonally crosslinked hyaluronate-collagen hydrogel for suture-free corneal defect repair. *Biomaterials.* 2020;255:120176.
28. Scalcione C, Ortiz-Vaquerizas D, Said DG, et al. Fibrin glue as agent for sealing corneal and conjunctival wound leaks. *Eye (Lond).* 2018;32:463–466.
29. Zhao L, Shi Z, Sun X, et al. Natural dual-crosslinking bioadhesive hydrogel for corneal regeneration in large-size defects. *Adv Healthc Mater.* 2022;11:e2201576.
30. Shirzaei Sani E, Kheirkhah A, Rana D, et al. Sutureless repair of corneal injuries using naturally derived bioadhesive hydrogels. *Sci Adv.* 2019;5:eav1281.
31. Chandru A, Agrawal P, Ojha SK, et al. Human cadaveric donor cornea derived extra cellular matrix microparticles for minimally invasive healing/regeneration of corneal wounds. *Biomolecules.* 2021;11:532.
32. Chen Z, You J, Liu X, et al. Biomaterials for corneal bioengineering. *Biomed Mater.* 2018;13:032002.
33. Palchesko RN, Carrasquilla SD, Feinberg AW. Natural biomaterials for corneal tissue engineering, repair, and regeneration. *Adv Healthc Mater.* 2018;7:e1701434.
34. Muthukumar T, Song JE, Khang G. Biological role of gellan gum in improving scaffold drug delivery, cell adhesion properties for tissue engineering applications. *Molecules.* 2019;24:4514.
35. Bhalerao H, Koteswara KB, Chandran S. Levofloxacin hemihydrate in situ gelling ophthalmic solution: formulation optimization and in vitro and in vivo evaluation. *AAPS PharmSciTech.* 2019;20:272.
36. Janga KY, Tatke A, Balguri SP, et al. Ion-sensitive in situ hydrogels of natamycin bilosomes for enhanced and prolonged ocular pharmacotherapy: in vitro permeability, cytotoxicity and in vivo evaluation. *Artif Cells Nanomed Biotechnol.* 2018;46:1039–1050.
37. Tatke A, Dudhipala N, Janga KY, et al. In situ gel of triamcinolone acetate-loaded solid lipid nanoparticles for improved topical ocular delivery: tear kinetics and ocular disposition studies. *Nanomaterials (Basel).* 2018;9:33.
38. Agibayeva LE, Kaldybekov DB, Porfiryeva NN, et al. Gellan gum and its methacrylated derivatives as in situ gelling mucoadhesive formulations of pilocarpine: in vitro and in vivo studies. *Int J Pharm.* 2020;577:119093.
39. Sun J, Zhou Z. A novel ocular delivery of brinzolamide based on gellan gum: in vitro and in vivo evaluation. *Drug Des Devel Ther.* 2018;12:383–389.
40. Cristiano MC, Froio F, Mancuso A, et al. The Rheolaser Master™ and Kinexus Rotational Rheometer® to evaluate the influence of topical drug delivery systems on rheological features of topical poloxamer gel. *Molecules.* 2020;25:1979.
41. Gao B, Luo J, Liu Y, et al. Intratumoral administration of thermosensitive hydrogel co-loaded with norcantharidin nanoparticles and doxorubicin for the treatment of hepatocellular carcinoma. *Int J Nanomedicine.* 2021;16:4073–4085.
42. Thomasy SM, Raghunathan VK, Winkler M, et al. Elastic modulus and collagen organization of the rabbit cornea: epithelium to endothelium. *Acta Biomater.* 2014;10:785–791.
43. Manda MG, da Silva LP, Cerqueira MT, et al. Gellan gum-hydroxyapatite composite spongy-like hydrogels for bone tissue engineering. *J Biomed Mater Res A.* 2018;106:479–490.
44. Mi S, Dooley EP, Albon J, et al. Adhesion of laser in situ keratomileusis-like flaps in the cornea: effects of crosslinking, stromal fibroblasts, and cytokine treatment. *J Cataract Refract Surg.* 2011;37:166–172.
45. Gu S, Xing C, Han J, et al. Differentiation of rabbit bone marrow mesenchymal stem cells into corneal epithelial cells in vivo and ex vivo. *Mol Vis.* 2009;15:99–107.
46. Scott MA, Nguyen VT, Levi B, et al. Current methods of adipogenic differentiation of mesenchymal stem cells. *Stem Cells Dev.* 2011;20:1793–1804.
47. Espana EM, Birk DE. Composition, structure and function of the corneal stroma. *Exp Eye Res.* 2020;198:108137.
48. Joshi VP, Vaishnavi K S, Ojha SK, et al. A reliable animal model of corneal stromal opacity: development and validation using in vivo imaging. *Ocul Surf.* 2020;18:681–688.
49. Gupta N, Kalaivani M, Tandon R. Comparison of prognostic value of Roper Hall and Dua classification systems in acute ocular burns. *Br J Ophthalmol.* 2011;95:194–198.
50. Stevens LR, Gilmore KJ, Wallace GG, et al. Tissue engineering with gellan gum. *Biomater Sci.* 2016;4:1276–1290.
51. García MC, Alfaro MC, Muñoz J. Rheology of sheared gels based on low acyl-gellan gum. *Food Sci Technol Int.* 2016;22:325–332.
52. Gering C, Rasheed A, Koivisto JT, et al. Chemical modification strategies for viscosity-dependent processing of gellan gum. *Carbohydr Polym.* 2021;269:118335.
53. Chen H, Zhang Y, Ding P, et al. Bone marrow-derived mesenchymal stem cells encapsulated in functionalized gellan gum/collagen hydrogel for effective vascularization. *ACS Appl Bio Mater.* 2018;1:1408–1415.
54. França FM, Tenuti JG, Broglio IP, et al. Low- and high-viscosity bulk-fill resin composites: a comparison of microhardness, microtensile bond strength, and fracture strength in restored molars. *Acta Odontol Latinoam.* 2021;34:173–182.
55. Mouser VHM, Levato R, Mensinga A, et al. Bio-ink development for three-dimensional bioprinting of hetero-cellular cartilage constructs. *Connect Tissue Res.* 2020;61:137–151.
56. Oliveira E, Assunção-Silva RC, Ziv-Polat O, et al. Influence of different ECM-like hydrogels on neurite outgrowth induced by adipose tissue-derived stem cells. *Stem Cells Int.* 2017;2017:6319129.
57. Rada T, Carvalho PP, Santos TC, et al. Chondrogenic potential of two hASCs subpopulations loaded onto gellan gum hydrogel evaluated in a nude mice model. *Curr Stem Cell Res Ther.* 2013;8:357–364.
58. Peris-Martínez C, García-Domene MC, Penadés M, et al. Spectral transmission of the human corneal layers. *J Clin Med.* 2021;10:4490.
59. van den Berg TJ, Tan KE. Light transmittance of the human cornea from 320 to 700 nm for different ages. *Vis Res.* 1994;34:1453–1456.

60. Chen S, Mienaltowski MJ, Birk DE. Regulation of corneal stroma extracellular matrix assembly. *Exp Eye Res.* 2015;133:69–80.
61. Massoudi D, Malecaze F, Galiacy SD. Collagens and proteoglycans of the cornea: importance in transparency and visual disorders. *Cell Tissue Res.* 2016;363:337–349.
62. Liu Y, Li Z, Li J, et al. Stiffness-mediated mesenchymal stem cell fate decision in 3D-bioprinted hydrogels. *Burns Trauma.* 2020;8:tkaa029.
63. Zhang S, Espandar L, Imhof KM, et al. Differentiation of human adipose-derived stem cells along the keratocyte lineage in vitro. *J Clin Exp Ophthalmol.* 2013;4:11435.
64. Dos Santos A, Balayan A, Funderburgh ML, et al. Differentiation capacity of human mesenchymal stem cells into keratocyte lineage. *Invest Ophthalmol Vis Sci.* 2019;60:3013–3023.
65. Chen J, Zhang W, Backman LJ, et al. Mechanical stress potentiates the differentiation of periodontal ligament stem cells into keratocytes. *Br J Ophthalmol.* 2018;102:562–569.
66. Harkin DG, Foyn L, Bray LJ, et al. Concise reviews: can mesenchymal stromal cells differentiate into corneal cells? A systematic review of published data. *Stem Cells.* 2015;33:785–791.
67. Wagenbrenner M, Mayer-Wagner S, Rudert M, et al. Combinations of hydrogels and mesenchymal stromal cells (MSCs) for cartilage tissue engineering-A review of the literature. *Gels.* 2021;7:217.
68. Zhao X, Song W, Chen Y, et al. Collagen-based materials combined with microRNA for repairing cornea wounds and inhibiting scar formation. *Biomater Sci.* 2018;7:51–62.
69. Oh JY, Kim MK, Shin MS, et al. The anti-inflammatory and anti-angiogenic role of mesenchymal stem cells in corneal wound healing following chemical injury. *Stem Cells.* 2008;26:1047–1055.
70. Beeken LJ, Ting DSJ, Sidney LE. Potential of mesenchymal stem cells as topical immunomodulatory cell therapies for ocular surface inflammatory disorders. *Stem Cells Transl Med.* 2021;10:39–49.